Electronic Supplementary Material (ESI) for Faraday Discussions.

Supplementary Information: Adsorption and Vibrational Spectroscopy of CO on the Surface of MgO from Periodic Local Coupled-Cluster Theory

Hong-Zhou Ye*,† and Timothy C. Berkelbach*,†,‡

†*Department of Chemistry, Columbia University, New York, New York 10027, USA*

‡*Initiative for Computational Catalysis, Flatiron Institute, New York, NY 10010, USA*

E-mail: hzyechem@gmail.com; t.berkelbach@columbia.edu

Note:

1. figures and equations appearing in the main text will be referred to as "Fig. Mxxx" and "Eq. Mxxx" in this Supplementary Material document.

2. Further supplementary data can be found in the following Github repository

https://github.com/hongzhouye/supporting_data/tree/main/2023/arXiv%3A2309.14651

Contents

S1 Optimized geometries

The geometry optimization is performed at the DFT@PBE+D3[1,2] level of theory using Quantum Espresso[3,4] and the PAW pseudopotential[5] (the $[2s^2 2p^6]$ of Mg is treated as valence electrons). The bulk MgO lattice is first optimized, from which the (001) surface is built and then optimized both with and without the CO adsorbate. A vacuum of 16 Å is employed. MgO slab models with two, three, and four atomic layers are considered in this work. During the optimization, atoms in the first layer of the two-layer slab model and the first two layers of both the three-layer and the four-layer models are allowed to relax, while atoms in the remaining layer(s) are kept fixed to their bulk optimized positions. The optimized structures are provided in the Github repository and summarized in Table S1. Our choice of DFT method (PBE+D3) is seen to well-reproduce the bulk MgO structure from both ref 6 obtained computationally using DFT@revPBE+D4[7,8] and ref 9 obtained using XPD experiments. Due to the weak perturbation of CO to the surface, the surface structure is also well-predicted by PBE+D3, resulting in a geometry relaxation energy Δ_{geom} close to that in ref 6 and several previous reports.[10,11] However, PBE+D3 significantly underestimates the Mg-C distance and overestimates the adsorption energy. For this reason, in the main text we manually adjust the Mg-C distance to be 2.460 Å to match that from[6] to facilitate the comparison.

Table S1: Comparison of computational and experimental geometric and energetic parameters.

	Lat. const. (Å)	d(Mg-C) (Å)	Δ_{geom} (kJ/mol)	E_{ads} (kJ/mol)	Reference
PBE+D3	4.222	2.377	1.1	−29.5	this work
revPBE+D4	4.220	2.460	0.8	−20.0	ref 6
Experiment	4.217				ref 9

S2 DFT single point calculations

All other DFT calculations, including the binding curves shown in FIG. M2 and the vibrational frequencies shown in FIG. M3 (which are in turn derived from the PESs shown in **??** below), were performed based on the optimized geometries obtained above. The non-dispersion part of the DFT

energy was calculated using PySCF. The TS, XDM, and MBD dispersion corrections were calculated using Quantum Espresso with the norm-conserving Hartwigesen-Goedecker-Hutter pseudopotential.[12,13] The D2 and D3 dispersion corrections were calculated using the `simple-dftd3` code (https://github.com/dftd3/simple-dftd3). The D4 dispersion correction was calculated using the `dftd4` code (https://github.com/dftd4/dftd4).

S3 Wavefunction single point calculations

S3.1 Estimating errors from Gaussian basis sets and pseudopotentials

Table S2: Summary of the errors due to the employed Gaussian basis sets and pseudopotentials.

Source	Estimated error (kJ/mol)
Diffuse functions	0.1
Pseudopotentials	< 0.1
Semi-core electron correlation of Mg	0.2
Total	0.3

In addition to the errors arising from TDL and CBS limit extrapolation as discussed in the Sec. IIIA, there are three major sources of errors in the correlated calculations of E_{int}:

1. Basis sets augmentation with diffuse functions
2. Pseudopotentials
3. Mg semicore electron correlation

Our final estimates of these errors are summarized in Table S2 and detailed in what follows. All three sources combined give an error bar of about 0.3 kJ/mol, which is added to the MP2 error bar discussed in the main text.

Basis sets augmentation with diffuse functions. For weak interactions, the regular Gaussian basis sets need to be augmented by diffuse functions for correlated calculations. We augment the GTH-cc-pV*X*Z basis sets[14] (referred to as *X*Z henceforth) with one diffuse function per angular

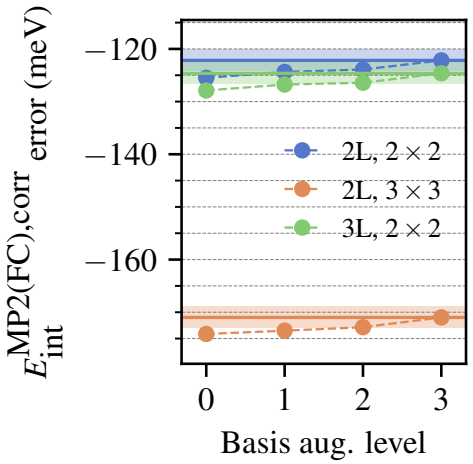

Figure S1: The correlation part of frozen-core MP2 interaction energy extrapolated to the CBS limit using TZ and QZ results for different choices of the basis set augmentation and slab models of different sizes. The shaded area indicates ±0.2 kJ/mol from the results obtained using level 3 basis set augmentation.

momentum channel to obtain the corresponding aug-GTH-cc-pV*X*Z basis sets (referred to as a*X*Z henceforth) for Mg, C, and O using the same protocol reported in ref 14. We generated fitting basis sets for both the augmented and the non-augmented Gaussian basis sets used in this work. All basis set data can be found in the Github repository.

Directly applying the a*X*Z basis sets to all atoms is unnecessary and also results in numerical problems due to the basis set linear dependency caused by the diffuse functions. We thus use a*X*Z basis sets only for the atoms near the adsorption center and monitor the convergence of the calculated interaction energy. Specifically, we define four levels of augmentation:

1. Level 0: using *X*Z basis sets for all atoms.

2. Level 1: using a*X*Z basis sets for the CO molecule.

3. Level 2: in addition to level 1, using a*X*Z basis sets for the surface Mg atom that binds CO.

4. Level 3: in addition to level 2, using a*X*Z basis sets for the four surface O atoms next to the Mg atom that binds CO.

In Fig. S1, we examine the effect of different augmentation levels for the MP2 interaction energy extrapolated to the CBS limit using TZ and QZ results for slabs of different size. We use level 3 in our final calculations and take the difference between the results from level 2 and level 3 as our estimated error, which is about 0.2 kJ/mol.

Table S3: HF and MP2 interaction energy for 2×2 and 3×3 surfaces calculated using both the GTH pseudopotential (optimized for HF) and the all-electron potential. The $1s^2$ core electrons in all atoms (Mg, C, and O) are frozen in the all-electron MP2 calculations to match the number of electrons in the GTH pseudopotential. All calculations were performed using the level 3 basis set augmentation scheme.

Surface	Basis set	$E_{\text{int}}^{\text{HF,All-e}}$	$E_{\text{int}}^{\text{HF,GTH}}$	$E_{\text{int}}^{\text{MP2,All-e}}$	$E_{\text{int}}^{\text{MP2,GTH}}$
2×2	DZ	4.9	4.6	−3.6	−3.8
	TZ	3.9	3.9	−7.5	−7.6
	QZ	3.7	3.8	−8.9	−8.9
	CBS(TZ,QZ)	3.7	3.8	−9.8	−9.8
3×3	DZ	3.1	2.8	−9.7	−10.0
	TZ	2.2	2.2	−13.9	−14.0
	QZ	2.1	2.2	−15.4	−15.4
	CBS(TZ,QZ)	2.1	2.2	−16.3	−16.4

Pseudopotential errors. The error introduced by using the GTH pseudopotentials is examined by comparison with calculations using the all-electron potential and Dunning's (aug-)cc-pVXZ basis sets.[15,16] The results are presented in Table S3 for different basis set size and surface size. We see that the at the CBS limit, the error caused by using the GTH pseudopotentials is less than 0.1 kJ/mol for both HF and MP2.

Table S4: HF and MP2 interaction energy for a 2×2 surfaces calculated using both the regular GTH-cc-pVXZ basis sets and the GTH-cc-pCVXZ basis sets with the GTH-HF pseudopotential. No electrons are frozen in the MP2 calculations. All calculations were performed using the level 3 basis set augmentation scheme.

Surface	Basis set	$E_{\text{int}}^{\text{HF}}$	$E_{\text{int}}^{\text{HF,core}}$	$E_{\text{int}}^{\text{MP2}}$	$E_{\text{int}}^{\text{MP2,core}}$
2×2	DZ	4.9	4.8	−3.6	−3.8
	TZ	3.9	3.8	−7.5	−7.8
	QZ	3.7	3.6	−8.9	−9.1
	CBS(TZ,QZ)	3.7	3.6	−9.8	−9.9

Correlation from semicore electrons of Mg. The $[2s^2 2p^6]$ semicore electrons of Mg may con-

tribute significantly to the interaction energy. To quantify this, we augment our (aug-)GTH-cc-pVXZ with core-correlating functions from the all-electron cc-pCVXZ basis sets.[17] The interaction energy evaluated with and without the core-correlating functions are listed in Table S4. We see that at the CBS limit the error due to using the regular (aug-)GTH-cc-pVXZ basis sets is about 0.2 kJ/mol for the MP2 interaction energy.

S3.2 Convergence with the MgO slab thickness

Table S5: HF and MP2 interaction energy for a 2×2 surfaces with different slab thickness. No electrons are frozen in the MP2 calculations. All calculations were performed using the level 3 basis set augmentation scheme.

Surface	Basis set	$E_{\text{int}}^{\text{HF,2L}}$	$E_{\text{int}}^{\text{HF,3L}}$	$E_{\text{int}}^{\text{MP2,2L}}$	$E_{\text{int}}^{\text{MP2,3L}}$
2×2	DZ	4.9	4.9	−3.6	−4.1
	TZ	3.9	3.7	−7.5	−7.9
	QZ	3.7	3.7	−8.9	−9.2
	CBS(TZ,QZ)	3.7	3.7	−9.8	−10.1

In Table S5, we compare the HF and MP2 interaction energy calculated for the 2-layer and 3-layer slab models. At the CBS limit, the difference between using the two slab models is negligible for HF and about 0.3 kJ/mol for MP2. Given the small energy differences and the higher computational expenses of using the thicker slabs, we use the 2-layer slab model for all calculations reported in the main text.

S3.3 Transferability of the $\Delta^{\text{CC(FC)}}(\eta)$ term

To examine the transferability of the correction term, $\Delta^{\text{CC(FC)}}(\eta)$, defined in eqn (M7) economically evaluated using the DF basis set and 2×2 surface, in Fig. S2 we show the η-convergence of the LNO-CCSD/CCSD(T) interaction energy for a larger surface of size 3×3. We see that $\Delta^{\text{CC(FC)}}(\eta)$ is as effective at accelerating the η-convergence for the larger surface as for the smaller one shown in FIG. M1E for both LNO-CCSD and LNO-CCSD(T). We hence apply $\Delta^{\text{CC(FC)}}(\eta)$ to all the LNO-CCSD/CCSD(T) calculations reported in the main text.

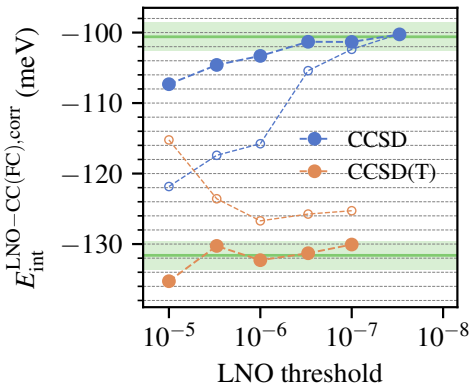

Figure S2: Same plot as FIG. M1E but for a 3×3 surface with the DZ basis set, with hollow and filled circles denoting uncorrected and corrected results, respectively.

S4 Potential energy surface and vibrational frequency

S4.1 PES fitting

For each method discussed in Sec. IIIC, we perform 130 single point energy calculations for d(C-O) from 0.982 to 1.432 Å with an increment of 0.05 Å and D(Mg-CO) from 2.630 to 3.830 Å with an increment of 0.1 Å. We fit the energy data using an n-th order polynomial

$$E(d, D; n) = \sum_{m=0}^{n} \sum_{p=0}^{m} a_{mp}^{(n)} d^p D^{m-p} \tag{S1}$$

From the fitted PES, the vibrational frequency can be calculated by diagonalizing the analytical Hessian evaluated at equilibrium (d_0, D_0). In Fig. S3, we show the fitting error of polynomial order $n = 4 - 8$ for the PBE+D3(0), MP2, CCSD, and CCSD(T) PES, calculated using the QZ basis set and the 3×3 surface. The vibrational frequency shift calculated for these PESs are plotted in Fig. S4. Based on these results, we identify $n = 6$ as the optimal choice that achieves both accurate fitting (with a maximum fitting error less than 0.5 kJ/mol) and stable frequency shift. We separately verified that fitting the one-dimensional PES for the free CO molecule with a 6-th order polynomial leads to $\nu_{\mathrm{CO(g)}}$ that agrees with that calculated using ORCA [18] based on analytical Hessians. In the following we fix $n = 6$ and study the convergence with respect to basis set size and surface size.

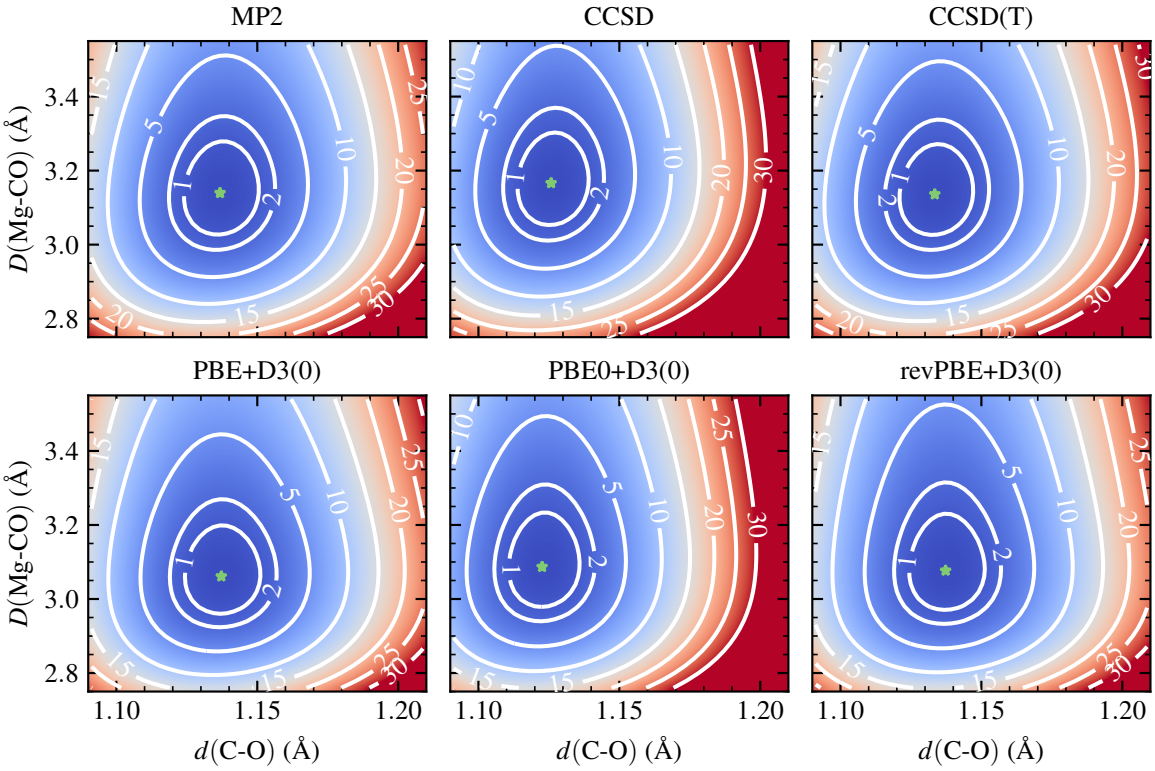

Figure S3: Error of the polynomial fitted PES (S1) of different polynomial order for PBE+D3(0), MP2, CCSD, and CCSD(T).

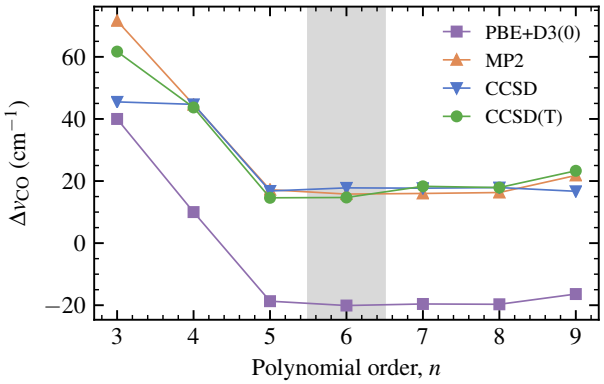

Figure S4: Convergence of the vibrational frequency shift with the polynomial order n used to fit the two-dimensional PES for evaluating $\nu_{\mathrm{CO(ads)}}$.

S4.2 Basis set, surface size, and LNO subspace

Table S6 shows the convergence of PBE and MP2 $\Delta\nu_{CO}$ with respect to the surface size and basis set size. From the table, we determine that the QZ basis set and 3×3 surface is suitable for all calculations.

Table S6: CO stretching frequency shift (in cm^{-1}) upon adsorption calculated using PBE and MP2 for different surface size and basis sets. QZ basis set and 3×3 surface are sufficient for a converged frequency calculation.

Surface	Basis set	PBE	MP2
3×3	DZ	−12.7	24.9
3×3	TZ	−20.6	17.2
3×3	QZ	−20.2	15.8
4×4	DZ	−12.7	24.9

Table S7 shows the η-convergence of the LNO-CCSD and LNO-CCSD(T) predicted frequency shift, from which we see that $\eta = 3 \times 10^{-6}$ converges $\Delta\nu_{CO}$ to within one wavenumber. The final CCSD/CCSD(T) frequency shift reported in the main text is calculated using 3×3/QZ energy obtained by the 3×3/TZ energy composite corrected by the difference between 2×2/TZ and 2×2/QZ.

Table S7: η-convergence of CO stretching frequency shift (in cm^{-1}) upon adsorption calculated using LNO-CCSD and LNO-CCSD(T) for two choices of surface size/basis set size: 2×2/TZ and 3×3/DZ. $\eta = 3 \times 10^{-6}$ is seen to reach convergence within one wavenumber for both cases.

Surface/basis	η	CCSD	CCSD(T)
2×2/TZ	1E-5	39.6	19.7
	3E-6	29.1	23.5
	1E-6	28.4	24.4
	3E-7	28.5	22.9
3×3/DZ	1E-5	27.6	23.4
	3E-6	26.0	23.2
	1E-6	25.1	23.7

S4.3 Final PES

The final PES obtained using the protocols discussed above are shown in Fig. S5 for different methods.

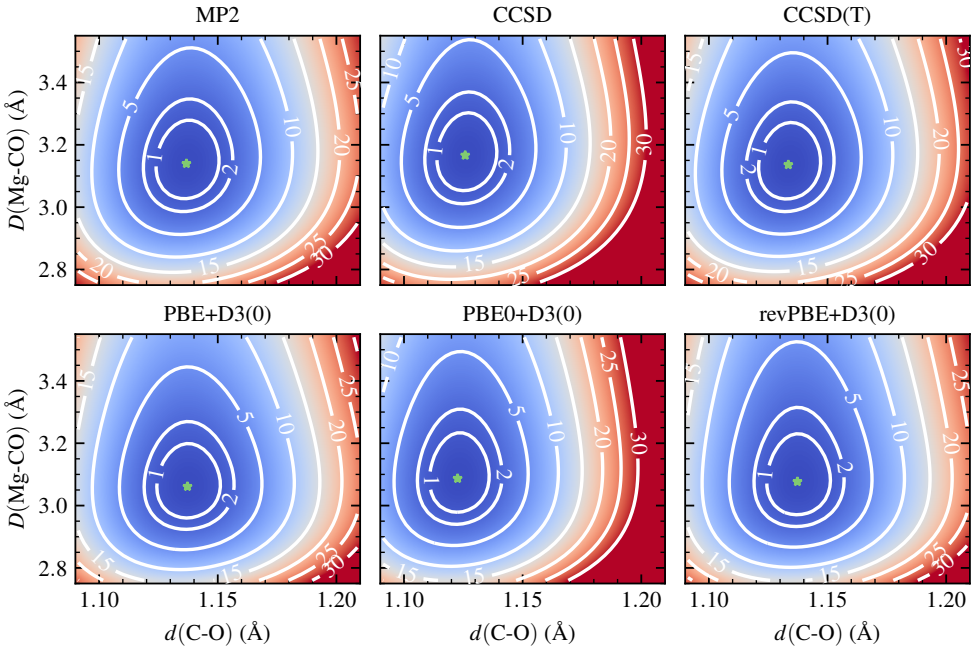

Figure S5: Same PES contour plot as in FIG. M3A for different methods.

References

(1) Perdew, J. P.; Burke, K.; Ernzerhof, M. Generalized Gradient Approximation Made Simple. *Phys. Rev. Lett.* **1996**, *77*, 3865–3868.

(2) Grimme, S.; Antony, J.; Ehrlich, S.; Krieg, H. A consistent and accurate ab initio parametrization of density functional dispersion correction (DFT-D) for the 94 elements H-Pu. *J. Chem. Phys.* **2010**, *132*, 154104.

(3) Giannozzi, P.; Baroni, S.; Bonini, N.; Calandra, M.; Car, R.; Cavazzoni, C.; Ceresoli, D.; Chiarotti, G. L.; Cococcioni, M.; Dabo, I.; Corso, A. D.; de Gironcoli, S.; Fabris, S.; Fratesi, G.; Gebauer, R.; Gerstmann, U.; Gougoussis, C.; Kokalj, A.; Lazzeri, M.; Martin-Samos, L.; Marzari, N.; Mauri, F.; Mazzarello, R.; Paolini, S.; Pasquarello, A.; Paulatto, L.; Sbraccia, C.; Scandolo, S.; Sclauzero, G.; Seitsonen, A. P.; Smogunov, A.; Umari, P.; Wentzcovitch, R. M. QUANTUM ESPRESSO: a modular and open-source software project for quantum simulations of materials. *J. Phys. Condens. Matter* **2009**, *21*, 395502.

(4) Giannozzi, P.; Andreussi, O.; Brumme, T.; Bunau, O.; Nardelli, M. B.; Calandra, M.; Car, R.; Cavazzoni, C.; Ceresoli, D.; Cococcioni, M.; Colonna, N.; Carnimeo, I.; Corso, A. D.; de Gironcoli, S.; Delugas, P.; DiStasio, R. A.; Ferretti, A.; Floris, A.; Fratesi, G.; Fugallo, G.; Gebauer, R.; Gerstmann, U.; Giustino, F.; Gorni, T.; Jia, J.; Kawamura, M.; Ko, H.-Y.; Kokalj, A.; Küçükbenli, E.; Lazzeri, M.; Marsili, M.; Marzari, N.; Mauri, F.; Nguyen, N. L.; Nguyen, H.-V.; de-la Roza, A. O.; Paulatto, L.; Poncé, S.; Rocca, D.; Sabatini, R.; Santra, B.; Schlipf, M.; Seitsonen, A. P.; Smogunov, A.; Timrov, I.; Thonhauser, T.; Umari, P.; Vast, N.; Wu, X.; Baroni, S. Advanced capabilities for materials modelling with Quantum ESPRESSO. *J. Phys. Condens. Matter* **2017**, *29*, 465901.

(5) Blöchl, P. E. Projector augmented-wave method. *Phys. Rev. B* **1994**, *50*, 17953–17979.

(6) Shi, B.; Zen, A.; Kapil, V.; Nagy, P.; Grüneis, A.; Michaelides, A. A coming of age for many-

body methods: Achieving consensus with experiments for CO on MgO. *Chemrxiv preprint* **2023**,

(7) Zhang, Y.; Yang, W. Comment on "Generalized Gradient Approximation Made Simple". *Phys. Rev. Lett.* **1998**, *80*, 890–890.

(8) Caldeweyher, E.; Bannwarth, C.; Grimme, S. Extension of the D3 dispersion coefficient model. *J. Chem. Phys.* **2017**, *147*, 034112.

(9) Lazarov, V. K.; Plass, R.; Poon, H.-C.; Saldin, D. K.; Weinert, M.; Chambers, S. A.; Gajdardziska-Josifovska, M. Structure of the hydrogen-stabilized MgO(111)−(1 × 1) polar surface: Integrated experimental and theoretical studies. *Phys. Rev. B* **2005**, *71*, 115434.

(10) Boese, A. D.; Sauer, J. Accurate adsorption energies of small molecules on oxide surfaces: CO–MgO(001). *Phys. Chem. Chem. Phys.* **2013**, *15*, 16481–16493.

(11) Alessio, M.; Usvyat, D.; Sauer, J. Chemically Accurate Adsorption Energies: CO and H2O on the MgO(001) Surface. *J. Chem. Theory Comput.* **2019**, *15*, 1329–1344.

(12) Goedecker, S.; Teter, M.; Hutter, J. Separable dual-space Gaussian pseudopotentials. *Phys. Rev. B* **1996**, *54*, 1703–1710.

(13) Hartwigsen, C.; Goedecker, S.; Hutter, J. Relativistic separable dual-space Gaussian pseudopotentials from H to Rn. *Phys. Rev. B* **1998**, *58*, 3641–3662.

(14) Ye, H.-Z.; Berkelbach, T. C. Correlation-Consistent Gaussian Basis Sets for Solids Made Simple. *J. Chem. Theory Comput.* **2022**, *18*, 1595–1606.

(15) Dunning, J., Thom H. Gaussian basis sets for use in correlated molecular calculations. I. The atoms boron through neon and hydrogen. *J. Chem. Phys.* **1989**, *90*, 1007–1023.

(16) Kendall, R. A.; Dunning, T. H.; Harrison, R. J. Electron affinities of the first-row atoms revisited. Systematic basis sets and wave functions. *J. Chem. Phys.* **1992**, *96*, 6796–6806.

(17) Woon, D. E.; Dunning, T. H. Gaussian basis sets for use in correlated molecular calculations. V. Core-valence basis sets for boron through neon. *J. Chem. Phys.* **1995**, *103*, 4572–4585.

(18) Neese, F.; Wennmohs, F.; Becker, U.; Riplinger, C. The ORCA quantum chemistry program package. *J. Chem. Phys.* **2020**, *152*, 224108.